Contact inhibitory Eph signalling decouples EGFR activity from vesicular recycling to generate contextual plasticity

Wayne Stallaert[1], Ola Sabet[1], Yannick Brüggemann[1,2], Lisa Baak[1] and Philippe I.H. Bastiaens[1,2*]

Affiliations

[1]Department of Systemic Cell Biology, Max Planck Institute of Molecular Physiology, Otto-Hahn-Str.11, 44227 Dortmund, Germany

[2]Faculty of Chemistry and Chemical Biology, TU Dortmund, Otto-Hahn-Str. 6, 44227 Dortmund, Germany

*Correspondence to: philippe.bastiaens@mpi-dortmund.mpg.de

Abstract

The ability of cells to adapt their behaviour to growth factors in relation to their environment is an essential aspect of tissue development and homeostasis. Here we show that cell-cell contact can change the outcome of EGFR activation by altering its vesicular trafficking. EGFR promotes Akt-mediated vesicular recycling to maintain its plasma membrane (PM) abundance during EGF stimulation. This self-sustained vesicular recycling of EGFR generates a positive feedback that maintains PM Akt signalling and promotes migration. By decoupling EGFR activation from its vesicular recycling, Eph activity at cell-cell contacts impedes the positive feedback that maintains PM signalling and traps EGFR in endosomes. Through this change in the spatial distribution of EGFR activity, cell-cell contact selectively suppresses migratory PI3K/Akt signalling from the PM, while preserving proliferative ERK signalling from endosomes. Thus, by altering the vesicular trafficking of EGFR, the cellular environment can modulate its signalling to generate diverse outcomes to EGF stimulation.

30
31
32
33 **Introduction**
34 Activation of epidermal growth factor receptor (EGFR) promotes a variety of cellular
35 responses including cell growth, proliferation, survival, apoptosis, differentiation and
36 migration (Yarden and Sliwkowski 2001), some of which are functionally opposed. To
37 select among these diverse outcomes, the cell requires additional contextual information.
38 This context can be intrinsic (e.g. cell type or cell cycle stage), or extrinsic, in the form of
39 extracellular signals that provide information about the current (or past) environmental
40 context. Adaptability to a changing environment requires that extrinsic information be
41 integrated through mechanisms that can transform the response to subsequent EGF
42 stimulation.
43
44 Vesicular trafficking allows the cell to enact a precise and coordinated response to
45 extracellular signals by dynamically regulating the spatial distribution of cell surface
46 receptors between the plasma membrane (PM) and functionally heterogeneous endosomal
47 compartments (Baumdick et al. 2015). Recycling of unliganded, monomeric EGFR through
48 the protein tyrosine phosphatase (PTP)-rich perinuclear environment safeguards against
49 autonomous receptor activation and regulates the cellular responsiveness to both new and
50 sustained stimuli by maintaining PM receptor abundance (Baumdick et al. 2015). EGF
51 binding promotes receptor ubiquitination (Sigismund et al. 2013), which re-routes
52 internalized EGFR to lysosomal degradation (Baumdick et al. 2015). Therefore, at
53 subsaturating EGF concentrations typically found in human tissue secretions (0.4-20
54 ng/ml)(Konturek et al. 1989), the cell maintains its sensitivity to persistent stimulation by
55 continually recycling unliganded, non-ubiquitinated receptors to the PM. Saturating EGF
56 concentrations (> 50 ng/ml)(Macdonald and Pike 2008), on the other hand, generate a
57 finite temporal response by progressively depleting PM and total EGFR abundance through
58 ubiquitin-dependent lysosomal degradation.
59

60 Although endocytosis reduces receptor activation and signalling at the PM, many receptors
61 continue to signal from endosomes following internalization (Villaseñor, Kalaidzidis, and
62 Zerial 2016; Sorkin and von Zastrow 2009; Daaka et al. 1998; Wouters and Bastiaens 1999;
63 DeFea et al. 2000; Maminska et al. 2016; Ménard, Parker, and Kermorgant 2014; Sadowski
64 et al. 2013; Howe et al. 2001; Verma et al. 2015). The signalling repertoire of these
65 endosomal receptors can differ from that at the PM if biochemical components of the
66 transduction machinery are not equally accessible in these distinct subcellular
67 environments. EGFR can continue to activate ERK1/2, for example, by scaffolding
68 components of this kinase cascade on endosomes (Guglielmo et al. 1994; Teis et al. 2006;
69 Nada et al. 2009; Fortian and Sorkin 2014; Villaseñor et al. 2015). *De novo* activation of Akt
70 by endosomal EGFR, on the other hand, is limited by a deficiency of the phosphoinositide
71 PI(4,5)P_2 in endosomal membranes (Matsuda et al. 2001; Haugh and Meyer 2002), which is
72 phosphorylated to PI(3,4,5)P_3 through the EGFR-mediated activation of phosphoinositide 3
73 kinase (PI3K) and acts as a docking site for Akt and its upstream kinase PDK1.
74 Consequently, sustained activation of Akt requires a continuous recycling of internalized
75 receptors to the PI(4,5)P_2-rich environment of the PM (Nishimura et al. 2015). Any changes
76 in EGFR trafficking dynamics which alter the distribution of receptors between the PM and
77 endosomal compartments might therefore change the signalling response to EGF
78 stimulation. Furthermore, recent evidence suggests that certain signalling molecules
79 downstream of cell surface receptors can, in turn, influence vesicular trafficking (Er et al.
80 2013; Laketa et al. 2014), generating a reciprocal relationship between receptor activation
81 and vesicular dynamics whose role in shaping the cellular response to stimuli has recently
82 begun to garner attention (Schmid 2017).
83
84 Given the role of trafficking in the regulation of EGFR activation and signalling, changes in
85 its vesicular dynamics may represent a mechanism through which the environmental
86 context can influence the cellular response to EGF stimulation. In the current work, we
87 reveal that cell-cell contact, through the activation of Eph receptors, selectively suppresses
88 EGF-promoted migratory signalling while preserving its proliferative response by altering
89 EGFR vesicular trafficking dynamics.
90

91 **Results**

92

93 *Akt-dependent recycling of EGFR sustains its autocatalytic activation at the PM*

94

95 In the absence of EGF stimulation, constitutive vesicular recycling of EGFR acts as a
96 safeguard against autonomous receptor activation both by reducing PM abundance and
97 continuously recycling receptors through the PTP-rich perinuclear compartment to
98 dephosphorylate the autocatalytic Y_{845} (Baumdick et al. 2015). We observed that this
99 constitutive recycling of unliganded EGFR is dependent on cellular Akt activity (**Fig. 1a-d**).
100 Endosomal accumulation of EGFR (**Fig. 1a, Supplementary Movie 1**) and a decrease in PM
101 EGFR abundance (**Fig. 1b top**) were observed following pharmacological inhibition of Akt
102 (**Fig. 1b bottom**) in Cos-7 cells. Consistent with a previous report, we found that Akt
103 inhibition traps endocytic EGFR in Rab5-positive early endosomes (**Fig. 1c**)(Er et al. 2013).
104 Conversely, an increase in Akt activation following inhibition of its negative regulator,
105 PP2A, by okadaic acid promoted a coincidental increase in the abundance of PM EGFR (**Fig.**
106 **1d**), demonstrating that the PM density of EGFR is positively regulated by Akt activity.

107

108 EGF binding increases the probability of EGFR ubiquitination (Sigismund et al. 2013),
109 which redirects liganded, internalized receptors toward the Rab7-positive late endosomal
110 compartment *en route* to degradation in the lysosome, while unliganded, non-ubiquitinated
111 receptors are recycled back to the PM (Baumdick et al. 2015). Since EGFR activation itself
112 increases Akt activity in cells (**Supplementary Fig. 1**), we asked whether the vesicular
113 recycling of unliganded receptors is increased during subsaturating EGF stimulation. By
114 measuring the accumulation of EGFR-paGFP at the PM following photoactivation in
115 endosomes (**Fig. 1e top**), we observed that EGF stimulation increased EGFR recycling (**Fig.**
116 **1e bottom**), while Akt inhibition suppressed EGFR recycling both prior to and during EGF
117 stimulation (**Fig. 1e**). Thus, through the activation of Akt, EGFR actively maintains its PM
118 abundance during persistent, subsaturating stimulation by increasing vesicular recycling.
119 Furthermore, by trapping internalized EGFR in Rab5-positive early endosomes, Akt
120 inhibition also impaired the transition of EGFR to Rab7-positive late endosomes (Poteryaev
121 et al. 2009) in EGF-stimulated cells (**Fig. 1c**), leading to a decrease in receptor degradation

122 (**Fig. 1f**). Therefore, by impeding trafficking from the early endosomal compartment, Akt
123 regulates both the recycling of unliganded, non-ubquitinated receptors to the PM and the
124 degradation of liganded, ubiquitinated receptors in the lysosome.
125
126 We next investigated how these effects of Akt on EGFR vesicular trafficking influence
127 receptor response properties during EGF stimulation. By decreasing PM receptor
128 abundance prior to and during EGF stimulation (**Fig. 1b,e**), pretreatment with an Akt
129 inhibitor significantly decreased the proportion of phosphorylated receptors at the
130 autocatalytic Y_{845}, the effector docking site Y_{1068} and the Cbl-mediated ubiquitination
131 regulatory site Y_{1045} (Baumdick et al. 2015) following 30 min of sustained EGF stimulation
132 (**Fig. 1g**). At higher EGF concentrations (≥ 50 ng/ml), Akt inhibition also suppresses
133 receptor degradation (**Fig. 1f**), trapping internalized EGFR in endosomal compartments
134 accessible to ER-bound PTPs with high activity (Yudushkin et al. 2007; Haj et al. 2002),
135 further decreasing the proportion of phosphorylated receptors in the entire cell (**Fig. 1g**).
136
137 At subsaturating, physiological EGF concentrations, EGFR phosphorylation is propagated at
138 the PM through the transphosphorylation of unliganded receptors by liganded receptors,
139 generating an autocatalytic activation of EGFR (Reynolds et al. 2003; Ibach et al. 2015;
140 Masip et al. 2016, Stanoev et al. 2017). Once unliganded receptors are phosphorylated on
141 $Y_{845,}$ which stabilizes their active conformation (Baumdick et. al, 2017), autocatalytic
142 activation can further propagate to additional unliganded EGFR. This autocatalytic
143 component in EGFR activation increases non-linearly with PM receptor density. We
144 therefore hypothesized that Akt activity might regulate EGFR autocatalysis by controlling
145 receptor abundance at the PM. As receptor occupancy increases at higher EGF
146 concentrations, EGFR phosphorylation becomes less dependent on autocatalysis.
147 Therefore, to specifically measure the effect of Akt on EGFR autocatalytic activation, we
148 stimulated cells with increasing, subsaturating concentrations of EGF-Alexa647 (1, 3, 10
149 and 20 ng/ml) and simultaneously measured EGF binding and EGFR activation (by
150 translocation of the EGFR phospho-tyrosine binding (PTB) domain) at the PM in individual
151 cells by time lapse imaging (**Fig. 1h-j**, **Supplementary Fig. 2**). Compared to control cells
152 (**Fig. 1h**), pretreatment with an Akt inhibitor decreased both EGF binding and EGFR

153 phosphorylation (**Fig. 1i**), consistent with a reduction in PM receptor abundance prior to
154 EGF stimulation (**Fig. 1b,e**). Plotting the relationship between the number of liganded
155 receptors (i.e. EGF-Alexa647 binding) and the extent of EGFR phosphorylation revealed
156 that phosphorylation increases non-linearly with EGF binding above a certain threshold in
157 control cells, consistent with an autocatalytic activation (**Fig. 1j**). Pretreatment with an Akt
158 inhibitor, on the other hand, generated less PM EGFR phosphorylation for equivalent
159 numbers of liganded receptors by impeding its autocatalytic activation (**Fig. 1j**). Therefore,
160 by promoting the constitutive recycling of EGFR to maintain its PM density prior to EGF
161 stimulation (**Fig. 1a-e**), Akt activity fosters the autocatalytic activation of EGFR at
162 subsaturating EGF concentrations.
163
164 Since EGF stimulation itself increases Akt-dependent vesicular recycling (**Fig. 1e**), we
165 further reasoned that EGFR might self-sustain its activation during persistent,
166 subsaturating EGF stimulation. To further investigate how Akt-dependent recycling
167 influences PM EGFR autocatalytic activation during EGF stimulation, measurements of
168 EGFR phosphorylation and trafficking were obtained by immunofluorescence prior to and
169 following subsaturating EGF stimulation (20 ng/ml) for 5, 30 and 60 min. Cells were
170 radially segmented to quantify changes in the spatial distribution of EGFR with time and
171 visualized using 3D spatial-temporal maps (**Fig. 1k,** Stanoev et al. 2017). By reducing PM
172 receptor density prior to EGF stimulation (**Fig. 1k, top**), pretreatment with an Akt inhibitor
173 decreased the proportion of phosphorylated EGFR at the PM after 5 min of EGF stimulation
174 (**Fig. 1k, bottom**), consistent with reduced EGFR autocatalysis (**Fig. 1j**). By continually
175 delivering internalized, non-ubiquitinated receptors to the PM to both bind additional EGF
176 and act as a substrate for autocatalysis, the EGF-induced increase in vesicular recycling
177 (**Fig. 1e**), maintains a high proportion of phosphorylated receptors at the PM during
178 sustained stimulation (**Fig. 1k, bottom**). Akt inhibition, on the other hand, by suppressing
179 the EGF-induced increase in receptor recycling (**Fig. 1e**) also reduced EGFR autocatalytic
180 activation at the PM at later time points (**Fig. 1k, bottom**) by trapping internalized
181 receptors in endosomes (**Fig. 1k, top**). Akt promotes vesicular trafficking through the
182 activation of the Rab5 effector PIKfyve (Er et al. 2013). PIKfyve inhibition led to an
183 endosomal accumulation of EGFR (**Supplementary Fig. 3a,b**) and decreased PM EGFR

184 abundance (**Fig. 1k, top**), consistent with a suppression of Akt-dependent recycling.
185 Decoupling Akt activation from its effect on trafficking by PIKfyve inhibition had
186 indistinguishable effects from direct Akt inhibition on EGFR phosphorylation and
187 trafficking (**Fig. 1l**), further validating that Akt activity sustains autocatalytic EGFR
188 activation at the PM through its effects on vesicular recycling.
189
190 Therefore, by stimulating an increase in Akt-dependent recycling, EGFR maintains its
191 sensitivity to EGF, effectively generating a positive feedback that sustains autocatalytic
192 EGFR activation at the PM during persistent, subsaturating stimulation (**Fig. 1l**).
193
194 *Eph receptor activation regulates EGFR vesicular trafficking*
195
196 The Eph family of receptor tyrosine kinases is activated at points of cell-cell contact
197 through interactions with membrane bound ephrin ligands presented on the surfaces of
198 adjacent cells (Pasquale 2010). Eph receptors, such as EphA2, in many ways operate in
199 functional opposition to EGFR, acting as a tumour suppressor (Miao et al. 2001; Batlle et al.
200 2005; Merlos-Suárez and Batlle 2008; Cortina et al. 2007; Li et al. 2009; Pasquale 2010;
201 Boyd, Bartlett, and Lackmann 2013) and mediating contact inhibition of locomotion to
202 suppress cellular migration and metastasis (Miao et al. 2009; Astin et al. 2010; Li et al.
203 2012; Lin et al. 2015). Indeed, a functional coupling of EGFR and Eph receptor activity has
204 recently been shown to regulate EGF-promoted migration (Lin et al. 2015). Since the
205 activation of Eph receptors decreases cellular Akt activity (**Supplementary Fig. 4a-b**)(Li et
206 al. 2012), we hypothesized that Eph receptors might regulate the cellular response to the
207 persistent, subsaturating EGF stimulation typical of pro-migratory signals by altering EGFR
208 vesicular trafficking.
209
210 Stimulation with soluble, clustered ephrinA1-Fc (A1)(Davis et al. 1994; Sabet et al. 2015),
211 led to Rab5-positive early endosomal accumulation of EGFR (**Fig. 2a-c, Supplementary**
212 **Movie 2**) and a reduction in PM EGFR abundance in Cos-7 (**Fig. 2d, Supplementary Fig.**
213 **4c-d**), HEK293 (**Supplementary Fig. 4e**), MCF10A (**Supplementary Fig. 4f**) and MDA-MB-
214 231 cells (**Supplementary Fig. 4g**). EGFR also accumulated in endosomes upon

215 physiological presentation of ephrinA1 ligand at sites of cell-cell contact (**Supplementary**
216 **Movie 3**). Consistent with the delayed endosomal accumulation of EGFR relative to EphA2
217 (**Fig. 2b,d**), we confirmed that the loss of PM EGFR does not result from the increased
218 formation of a heterodimer (**Supplementary Fig. 5**) or through the transactivation of
219 EGFR by EphA2 (**Fig 2e**). To directly assess whether Eph receptors decrease PM EGFR
220 through an inhibition of Akt-mediated EGFR recycling, we stimulated cells for 15 min with
221 a subsaturating concentration of EGF to induce EGFR endocytosis and measured the
222 subsequent recycling of internalized receptors back to the PM after EGF washout (**Fig. 2f**).
223 In control cells, the PM abundance of EGFR recovered to pre-EGF levels following washout,
224 while in A1-pretreated cells, EGFR recycling was significantly inhibited (**Fig. 2f**), consistent
225 with an EphA2-mediated inhibition of Akt-dependent recycling.
226
227
228 *Cell-cell contact alters the spatial distribution of EGFR activity*
229
230 We next assessed whether prior activation of Eph receptors regulates the subsequent
231 cellular response to EGF by suppressing its vesicular recycling. Similar to the effect of Akt
232 and PIKfyve inhibition (**Fig. 1k**), A1 pretreatment reduced autocatalytic activation of EGFR
233 at the PM during persistent, subsaturating EGF stimulation, while preserving EGFR
234 phosphorylation in endosomes (**Fig. 3a**). Although EGFR can continue to activate some
235 signalling effectors from endosomal membranes (Villaseñor, Kalaidzidis, and Zerial 2016;
236 Sorkin and von Zastrow 2009), Akt itself is preferentially activated at the PM
237 (**Supplementary Fig. 1**)(Haugh and Meyer 2002; Nishimura et al. 2015). By suppressing
238 the positive feedback that maintains EGFR activation at the PM, A1 pretreatment
239 selectively inhibited EGF-promoted Akt activation in both Cos-7 and HEK293 cells (**Fig. 3b**
240 **top, Supplementary Fig. 6**), while ERK activation, which can continue from endosomal
241 membranes (**Supplementary Fig. 1c-d**)(Guglielmo et al. 1994; Nada et al. 2009; Villaseñor
242 et al. 2015), remained intact (**Fig 3b bottom, Supplementary Fig. 6**). To confirm that
243 EphA2 inhibits EGF-promoted Akt activation by suppressing EGFR recycling and does not
244 simply reflect the opposed regulation of Akt by EGFR and EphA2 (activation vs inhibition,
245 respectively), we assessed whether EGFR trafficking was dispensable for the A1-induced

246 suppression of EGF-promoted Akt activation. Cells were prestimulated with A1 for 30
247 minutes, followed by treatment with the dynamin inhibitor dynole 34-2 to block
248 subsequent endocytosis, and then stimulated with EGF. When EGFR endocytosis was
249 blocked (**Supplementary Fig. 1c**), A1 pretreatment had no effect on EGF-promoted Akt
250 activation (**Fig. 3c top**), while the negative control analogue, dynole 31-2, which does not
251 inhibit EGFR endocytosis (**Supplementary Fig. 1c**), had no effect on A1-induced
252 suppression of EGF-promoted Akt activation (**Fig. 3c bottom**), corroborating that intact
253 EGFR vesicular trafficking is required for the inhibitory effect of Eph receptors on EGFR
254 signalling.
255
256 Increasing concentrations of A1 progressively inhibited EGF-mediated Akt activation (**Fig.**
257 **3d**), suggesting that the amount of ephrinA1:Eph receptor interactions at points of cell-cell
258 contact might determine the magnitude of Akt activation in response to a given
259 concentration of EGF. To directly investigate the influence of cell-cell contact on EGFR
260 signalling, we obtained single cell measurements of Akt and ERK activation in cells with
261 varying degrees of cell-cell contact (**Fig. 3e,f**). Akt activation decreased with cell-cell
262 contact both prior to (F = 16.0, p = 0.001, r^2 = 0.432) and following EGF stimulation (F =
263 21.4, p < 0.001, r^2 = 0.322) (**Fig. 3e**), demonstrating that increasing cell-cell contact reduces
264 the magnitude of EGF-promoted Akt activation. ERK activation, on the other hand, was
265 unaffected by cell-cell contact (unstimulated: F = 0.180, p = 0.673, r^2 = 0.003; EGF: F =
266 0.321, p = 0.575, r^2 = 0.009), with cells generating similar EGF-promoted increases in ERK
267 activation irrespective of their degree of cell-cell contact (**Fig. 3f**).
268
269 To determine whether environmental signals other than cell-cell contact can influence
270 EGFR signalling through changes in its vesicular trafficking, we investigated the effect of
271 prior activation of the G protein-coupled receptor Kiss1 (Kiss1R), which, similar to EphA2,
272 inhibits Akt and acts as a tumour and metastasis suppressor (Navenot, Fujii, and Peiper
273 2009). Stimulation with the Kiss1R ligand kisspeptin-10 (Kp-10) reduced Akt activity and
274 decreased PM EGFR abundance (**Fig. 3g**). Similar to the effect of cell-cell contact,
275 pretreatment with Kp-10 selectively inhibited EGF-promoted Akt activation (**Fig. 3h**),
276 while preserving ERK activation (**Fig. 3i**). Changes in EGFR vesicular trafficking dynamics,

277 therefore, provides a general mechanism to generate plasticity in the signalling response to
278 EGFR activation, through which diverse environmental signals such as cell-cell contact or
279 soluble stimuli like Kp-10 can influence the cellular response to EGF.
280
281 Positive feedback in combination with inhibitory network motifs can convert graded inputs
282 into switch-like, ultrasensitive signalling responses (Ferrell and Ha 2014). Since Akt is
283 preferentially activated at the PM (**Supplementary Fig. 1**), the EGF-induced increase in
284 EGFR vesicular recycling (**Fig. 1e**) should generate a positive feedback for Akt activation
285 (**Fig. 1l**). While population-based measurements of Akt activation do not demonstrate
286 ultrasensitivity (**Fig. 3d**, Hill coefficient of 0.975±0.215 for control cells), if cells possess
287 intrinsic variability in the EGF concentration required to stimulate Akt-dependent
288 recycling, ultrasensitivity in individual cells will be averaged out at the population level to
289 produce a graded response (Ferrell and Machleder 1998). To investigate if this positive
290 feedback can generate a switch-like activation of Akt at the single cell level, we measured
291 the Akt response in thousands of individual cells by flow cytometry following sustained
292 stimulation (60 min) with a range of EGF concentrations (0.25-100 ng/ml) (**Fig. 3j-k**).
293 Additionally, cells were stimulated in suspension to negate the effect of *in situ* cell-cell
294 contact as an extrinsic source of variability in Akt activation (**Fig. 3e**). At concentrations ≥ 1
295 ng/ml, EGF stimulation produced a switch-like activation to a high Akt phosphorylation
296 state in a subpopulation of cells, whose proportion increased with EGF concentration (**Fig.
297 3j-k, top**). Decoupling EGFR activation from its effect on vesicular recycling by PIKfyve
298 inhibition (**Fig. 3j-k, middle**) or A1 pretreatment (**Fig. 3j-k, bottom**) did not result in a
299 global decrease in Akt activation but rather reduced the proportion of cells generating a
300 high Akt response, consistent with an inhibition of the positive feedback that produces this
301 switch-like response. Intrinsic cell-to-cell variability in the EGF threshold required to
302 stimulate Akt-dependent vesicular recycling, therefore, determines the proportion of cells
303 that transition to a high Akt activity state at a given EGF concentration.
304
305 If the transition to a high Akt activity state is dependent on the positive feedback produced
306 by coupling EGFR activation to vesicular recycling, we should also observe similar cell-to-

307 cell variability in PM EGF binding during sustained stimulation. We therefore performed
308 single cell time lapse imaging and quantified PM EGF binding during persistent stimulation
309 with a subsaturating concentration of EGF-Alexa647 (20 ng/ml) (**Fig. 3l-n**). Cells that
310 successfully engage Akt-dependent recycling should exhibit a more sustained EGF binding
311 at the PM during stimulation. Cells were grouped by their rate of loss in PM EGF binding
312 using k-means clustering into two groups exhibiting a slow (Group 1) or fast (Group 2) loss
313 of PM EGF during stimulation (**Fig. 3l-m**). While cells of both types were observed in
314 control and A1 pretreated samples, in control conditions we observed an enrichment of
315 cells with sustained binding (Group 1; 28%) versus cells pretreated with A1 (10.5%) (**Fig.
316 3n**). Although the percent of cells generating sustained EGF binding in control cells (**Fig.
317 3n**) is less than the proportion producing a high Akt response in flow cytometry
318 experiments (**Fig. 3j-k, top**), *in situ* cell-cell contact during time lapse imaging should
319 decrease the number of cells stimulating Akt-dependent recycling, consistent with the
320 observed effect of Eph receptor activation (**Fig. 3j-k, bottom**).
321
322 Thus, cells possess intrinsic variability to engage Akt-dependent recycling and preserve PM
323 EGF binding during sustained stimulation. Eph receptor activation, by decoupling EGFR
324 activation from its effect on vesicular trafficking, reduces Akt activation within the
325 population by decreasing the proportion of cells transitioning to a high Akt activity state
326 during persistent EGF stimulation.
327
328 *Cell-cell contact changes the cellular outcome of EGF stimulation*
329
330 EGFR signalling to effectors at the PM generates exploratory cellular behaviours (Chinkers,
331 McKanna, and Cohen 1979; Ridley and Hall 1992; Chan et al. 1998; Segall et al. 1996; Bailly
332 et al. 1999; Harms et al. 2005; Yip et al. 2007; El-Sibai et al. 2007) that must be maintained
333 to induce a persistent migratory response. Given that contact inhibitory Eph receptor
334 activation selectively suppresses PM signalling during persistent, subsaturating EGF
335 presentation (**Fig. 3b,e,f**), we investigated if cell-cell contact regulates EGF-promoted
336 migration by inhibiting Akt-dependent recycling. NIH 3T3 mouse embryonic fibroblast
337 (MEF) cells were grown on fibronectin in the presence of a silicone barrier that, once

338 removed, creates a cell-free area into which individual cells can be tracked following
339 uniform stimulation with EGF. When grown on fibronectin in 2-D cultures, fibroblasts
340 generate an autonomous, haptotactic migratory response which is enhanced by an EGF-
341 induced increase in their exporatory behaviour (Li et al. 1999). Following stimulation with
342 subsaturating EGF concentrations (20 ng/ml), we observed a signficant increase in the
343 proportion of migratory cells (**Fig. 4a, top, Supplementary Movie 4, Supplementary Fig.**
344 **7**), but no change in the average distance travelled by migrating cells (**Fig. 4a, bottom**),
345 indicating that EGF promotes the transition of individual cells to a migratory state rather
346 than increasing overall cellular motility. Since ligand binding promotes receptor
347 ubiquitination and degradation, persistent stimulation with saturating, supraphysiological
348 EGF concentrations (100 ng/ml) induces a loss in EGF sensitivity with time and thus does
349 not significantly increase the proportion of migratory cells (**Fig. 4a, top**). Decoupling EGFR
350 activation from its effect on trafficking through the PIKfyve inhibition or A1 pretreatment
351 decreased the proportion of migratory cells (**Fig. 4a**), demonstrating that the positive
352 feedback generated by the EGF-induced increase in Akt-dependent recycling promotes the
353 transition to a migratory state. We observed further that increasing concentrations of A1
354 progressively decreased EGF-induced migration (**Fig. 4a**), consistent with its
355 concentration-dependent effect on EGF-promoted Akt activation (**Fig. 3d**) and suggesting
356 that the amount of ephrinA1-Eph receptor interactions at points of cell-cell contact may
357 determine whether a cell initiates a migratory response to EGF. Consistent with this
358 observation, we found that the number of migratory cells following EGF stimulation was
359 inversely proportional to cell density (**Fig. 4b**) and that the increase in migration observed
360 at low densities could be countered by treatment with soluble A1 to mimic Eph receptor
361 contact inhibitory signalling (**Fig. 4b**). Thus, physiological Eph receptor activation at points
362 of cell-cell contact suppresses EGF-promoted migration by inhibiting Akt-dependent
363 vesicular recycling. However, by preserving endosomal ERK activation following EGF
364 stimulation (**Fig. 3b, bottom**), we found that neither PIKfyve inhibition nor A1
365 pretreatment led to a reduction in EGF-promoted cell proliferation (**Fig. 4c**). Thus by
366 altering the spatiotemporal distribution of EGFR activity, contact inhibitory signalling by
367 Eph receptors determines the cellular outcome to EGF stimulation, biasing cells to a
368 proliferative instead of a migratory response.

369
370
371 **DISCUSSION**
372
373 In this paper, we demonstrate that cell-cell interactions can generate context-dependent
374 cellular outcomes to EGF stimulation by modulating EGFR vesicular trafficking dynamics.
375
376 Akt-dependent recycling promotes EGFR activation both by enriching the concentration of
377 potential EGF binding sites at the PM but also by increasing the autocatalytic activation of
378 unliganded receptors by transphosphorylation. By increasing Akt activity, EGF stimulation
379 generates a positive feedback that maintains EGFR density at the PM by increasing the
380 vesicular recycling of non-ubiquitinated receptors during persistent, subsaturating
381 stimulation (**Fig. 1e**). Saturating, supraphysiological EGF concentrations, on the other hand,
382 increase the proportion of liganded, ubiquitinated receptors that unidirectionally traffic, in
383 an Akt-dependent manner, from early to late endosomes to be degraded in lysosomes (**Fig.**
384 **1c,f**)(Baumdick et al. 2015), resulting in a depletion of PM EGFR abundance with time.
385 Chemotaxis requires that cells remain responsive to stimuli for prolonged periods of time
386 as they migrate toward the chemotactic source. Akt-dependent trafficking, therefore,
387 determines the concentration range at which EGF produces a migratory response. By
388 increasing both the vesicular recycling of unliganded, non-ubiquitinated receptors and the
389 degradation of ubiquitinated receptors, Akt activation maintains cellular sensitivity to
390 persistent, subsaturating EGF concentrations, while limiting the duration of receptor
391 activation to saturating concentrations.
392
393 Since Akt itself is preferentially activated at the PM (**Supplementary Fig. 1**), the EGF-
394 promoted increase in vesicular recycling generates a positive feedback that switches cells
395 to a high Akt activation state (**Fig. 3j-k**). Although Akt has been previously observed on
396 endosomal membranes through interactions with the early endocytic adaptor protein
397 APPL1 (Schenck et al. 2008; Ebner et al. 2017), *de novo* activation of Akt by EGFR requires
398 the production of PI(3,4,5)P_3, which is impeded by the low abundance of PI(4,5)P_2 in
399 endosomal membranes (Matsuda et al. 2001; Haugh and Meyer 2002). Although Akt

400 activation may occur to some extent on endosomal membranes (Jethwa et al. 2015), since
401 the coupling of active EGFR to Akt activation will be more efficient at the PM, any
402 perturbations that influence the spatial distribution of EGFR will influence the capacity of
403 EGFR to activate Akt (**Fig. 3b, Supplementary Fig. 1c**).
404
405 We observed that the switch to a high Akt activity state only occurs in a proportion of cells,
406 which increases with EGF concentration (**Fig. 3j-k**). Population heterogeneity in Akt
407 activation has been previously attributed to cell-to-cell variation in PI3K expression (Yuan
408 et al. 2011). Our data suggest that intrinsic variability in the expression of signalling and/or
409 trafficking effectors may determine, for a given cell, the EGF concentration required to
410 stimulate Akt-dependent trafficking and engage the positive feedback that produces a high
411 Akt activity state. Small differences in EGF concentration substantially influence the
412 proportion of cells generating a high Akt response (e.g. a shift from 5 to 10 ng/ml increases
413 the proportion of cells from 43 to 85%, respectively, **Fig. 3j-k**). Perhaps it is not
414 coincidental that the concentration range over which this switch occurs corresponds to the
415 physiological range of EGF concentrations in human tissue secretions (Konturek et al.
416 1989). By generating a sharp boundary for Akt activation within the physiological EGF
417 concentration regime, even slight changes in the threshold of this switch could have
418 profound implications for tissue dynamics (e.g. initiation of migration).
419
420 Eph receptor activation, for example, by suppressing EGFR recycling, decreased the
421 proportion of cells generating a high Akt response from 85 to 41% in response to 10 ng/ml
422 EGF (**Fig. 3j-k**). The dependence of Akt activation on EGFR recycling allows the degree of
423 cell-cell contact, or other environmental stimuli that influence vesicular dynamics, to
424 regulate proportion of cells generating a migratory response to EGF stimulation. PI3K/Akt
425 signalling has previously been suggested as the point of convergence for EGFR/EphB2
426 control of cell migration (Lin et al. 2015); however, the molecular mechanism underlying
427 this oppositional relationship remained unclear. Our results indicate that Eph receptor
428 activation inhibits EGF-promoted cell migration by suppressing Akt-dependent recycling,
429 thus impeding the positive feedback that generates a high Akt response and decreasing the
430 sensitivity of cells to persistent EGF stimulation necessary to maintain exploratory

431 behaviour. However, by changing the spatial distribution of active EGFR, Eph receptor
432 activation selectively suppresses migratory signalling from the PM while leaving
433 proliferative ERK signalling intact (**Fig. 3b,e-f, Fig. 4**)(Li et al. 2012). This contextual
434 plasticity generates two distinct cellular outcomes to EGF stimulation that may be
435 important in physiological settings such as wound healing. At the tissue boundary, cells
436 with reduced cell-cell contact would increase their exploratory behaviour in response to
437 EGF released at the site of the wound. Cells located deeper in the tissue, despite extensive
438 cell-cell contact, would retain their proliferative response to environmental EGF, and
439 undergo mitosis to fill the vacant space created as exploratory cells migrate to occupy the
440 wound area.
441
442 Our results suggest that the spatial component of the positive feedback generated by Akt-
443 dependent recycling may also explain how EGF can act as a positional chemotactic cue (e.g.
444 during *Drosophila* border cell migration)(Duchek and Rørth 2001). Given the small
445 difference in EGF concentration between the leading edge and the tail of a migrating cell in
446 a shallow EGF gradient, preferential trafficking of receptors to the PM region of highest
447 EGFR activity would enhance local signalling (Bailly et al. 2000) to enrich exploratory
448 behaviour in the direction of the EGF source (Jékely et al. 2005; Arrieumerlou and Meyer
449 2005), leading to directed movement.
450
451 Our observations demonstrate that crosstalk between receptors with opposed functionality
452 can emerge through changes in vesicular trafficking dynamics rather than relying on direct
453 interactions between the receptors or their respective effectors. Such a mechanism also
454 allows different receptors with similar functional roles (e.g. EphA2 and Kiss1R) to alter the
455 cellular response to stimuli without having to evolve distinct protein interaction domains
456 to do so. The dependency of EGFR signalling on its vesicular dynamics thus confers a
457 universal mechanism through which the cell can generate functional plasticity to growth
458 factor stimulation while preserving specificity in cell-cell communication through the
459 coexpression of distinct but functionally-related cell surface receptors.
460 **Acknowledgements**

The project was partially funded by the European Research Council (ERC AdG 322637) to P.I.H.B. We would like to thank Dr. Astrid Krämer for critically reading this manuscript, Dr. Aneta Koseska for assistance in data interpretation and analysis and Dr. Klaus Schuermann for help with data visualization.

Author contributions

P.I.H.B. and W.S. conceived the project. W.S. performed and analysed most experiments. O.S. contributed to the migration experiments, Y.B. contributed to the time lapse imaging of EGF binding, L.B. contributed to the ICW and immunoprecipitation experiments. W.S. wrote the manuscript with assistance from P.I.H.B.

Competing financial interests

The authors declare that no competing interests exist.

474 **Methods**

475

476 *Primary antibodies*

477 Mouse anti-Akt (2920, Cell Signalling Technology (CST), Danvers, MA, USA), mouse anti-
478 Akt-Alexa488 (2917, CST), rabbit anti-phospho-Akt(Ser473) (4060, CST), rabbit anti-
479 phospho-Akt (Ser473)-Alexa647 (4075, CST), mouse anti-HA (9658, Sigma-Aldrich,
480 St.Louis, MO, USA), rabbit anti-EGFR (4267, CST), goat anti-EGFR (AF231, R&D Systems,
481 Minneapolis, MN, USA), mouse anti-phospho-EGFR(Tyr845) (558381, BD Biosciences,
482 Heidelberg, Germany), rabbit anti-phospho-EGFR(Tyr1045) (2237, CST), mouse anti-
483 phospho-EGFR(Tyr1068) (2236, CST), goat anti-EphA2 (R&D Systems), rabbit anti-
484 phospho-Eph(Tyr588/596) (Abcam, Cambridge, UK), mouse anti-ERK1/2 (4696, CST),
485 rabbit anti-phospho-ERK(Thr202/Tyr204) (4370, CST), mouse anti-Rab5 (610724, BD
486 Biosciences), rabbit anti-Rab7 (9367, CST), rabbit anti-phospho-Rb(Ser807/811, CST)
487 mouse anti-tubulin (6074, Sigma-Aldrich)

488

489 *Secondary antibodies*

490 IRDye 680RD Donkey anti-Mouse (LI-COR Biosciences), IRDye 680RD Donkey anti-Rabbit
491 (LI-COR Biosciences), IRDye 680RD Donkey anti-Goat (LI-COR Biosciences), IRDye 800CW,
492 Donkey anti-Mouse (LI-COR Biosciences), IRDye 800CW Donkey anti-Rabbit (LI-COR
493 Biosciences), IRDye 800CW Donkey anti-Rabbit (LI-COR Biosciences), AlexaFluor 405 goat
494 anti-Mouse (Life Technologies), AlexaFluor 488 donkey anti-Goat (Life Technologies),
495 AlexaFluor 546 donkey anti-rabbit (Life Technologies), AlexaFluor 647 donkey anti-Rabbit
496 (Life Technologies)

497

498 *Plasmids*

499 Generation of EGFR-mCitrine, EGFR-mCherry, EGFR-paGFP, PTB-mCherry and HA-
500 ubiquitin (Baumdick et al. 2015), and EphA2-mCitrine (Sabet et al. 2015) were previously
501 described. pcDNA3.1-EphA2 was a gift from Tony Pawson.

502

503

504

505 *Reagents*

506 AktVIII (sc-3513, Santa Cruz Biotechnology, Dallas, TX, USA), EGF (AF-100-15, Peprotech,
507 Hamburg, Germany), okadaic acid (sc-3513, Santa Cruz Biotechnology), YM201636 (13576,
508 Biomol GmbH, Hamburg, Germany), dynole 31-2 (ab120464, Abcam), dynole 34-2
509 (ab120463, Abcam), Kisspeptin-10 (445888, Merck Millipore). EGF-Alexa647 was
510 prepared as previously described (Baumdick et al. 2015). EphrinA1-Fc (602-A1-200) was
511 preclustered by incubating with chicken Anti-Fc (GW200083F, Sigma-Aldrich) at a ratio of
512 5:1 at room temperature for at least 30 min.

513

514 *Cell culture*

515 Cos-7, HEK293 and NIH 3T3 cells were grown in Dulbecco's Modified Eagle's Medium
516 (DMEM) supplemented with 10% fetal bovine serum (FBS), 2 mM L-glutamine and 1%
517 non-essential amino acids (NEAA) and maintained at 37°C in 5% CO_2. MCF10A cells were
518 grown in DMEM/F12 supplemented with 5% horse serum, 20 ng/ml EGF, 500 ng/ml
519 hydrocortisone, 100 ng/ml cholera toxin and 10 µg/ml insulin and maintained at 37°C in
520 5% CO_2. MDA-MB-231 cells were grown in Leibowitz medium supplemented with 10%
521 FBS and 2mM L-glutamine maintained at 37°C in 0% CO_2. When required, transfection of
522 cells was performed using FUGENE6 (Roche Diagnostics, Mannheim, Germany) or
523 Lipofectamine 2000 (Life Technologies, Darmstadt, Germany) according to manufacturer's
524 protocol. Approximately 16-18 hours prior to an experiment, cells were starved in DMEM
525 containing 0.5% FBS, 2 mM L-glutamine and 1% NEAA. One hour before stimulation,
526 starvation media was changed to serum-free DMEM or DMEM without phenol red for live
527 cell imaging. Unless explicitly stated in the figure legends, all experiments were performed
528 with Cos-7 cells with endogenous expression of EGFR and Eph receptors.

529

530 *In-cell westerns (ICW) and on-cell westerns (OCW)*

531 Cells were seeded on black, transparent bottomed 96-well plates (3340, Corning, Hagen,
532 Germany) coated with poly-L-lysine (P6282, Sigma Aldrich). Cell were fixed with Roti-
533 Histofix 4% (Carl Roth, Karsruhe, Germany) for 5 min at 37°C. For ICW, cells were
534 permeabilized with 0.1% Triton X-100 (v/v) for 5 min at room temperature. For OCW, cells
535 were not permeabilized. Samples were incubated in Odyssey TBS blocking buffer (LI-COR

536 Biosciences, Lincoln, NE, USA) for 30 min at room temperature. Primary antibodies were
537 incubated overnight at 4°C and secondary antibodies (IRDyes, LI-COR Biosciences) were
538 incubated in the dark for 1 h at room temperature. All wash steps were performed with
539 TBS (pH 7.4). Intensity measurements were made using the Odyssey Infrared Imaging
540 System (LI-COR Biosciences). Quantification of the integrated intensity in each well was
541 performed using the MicroArray Profile plugin (OptiNav Inc., Bellevue, WA, USA) for ImageJ
542 v1.47 (http://rsbweb.nih.gov/ij/). In each ICW or OCW, 2-4 replicates per conditions were
543 obtained per experiment, and all data presented represents means ± s.e.m. from at least
544 three independent experiments.
545
546 *Immunofluorescence*
547 Cells were cultured on 4-well chambered glass slides (Lab-tek, Thermo Fisher Scientific,
548 Waltham, MA) and fixed with 4% paraformaldehyde/PBS (w/v) for 10 min at 4°C. To
549 measure PM EGFR, fixed, non-permeabilized samples were first incubated with primary
550 antibody directed at an extracellular epitope of EGFR (AF231, R&D Systems, 1:200)
551 overnight at 4°C followed by secondary antibody for 1 h at room temperature. For all other
552 immunofluorescence experiments, samples were permeabilized with 0.1% Triton X-100
553 (v/v) for 5 min at room temperature prior to incubation with primary antibodies. All wash
554 steps were performed with TBS (pH 7.4). Fixed samples were imaged in PBS at 25°C. For all
555 analysis, an initial background subtraction was performed on immunofluorescence images.
556 To quantify the proportion of EGFR in Rab5 and Rab7 compartments, binary masks were
557 generated from intensity thresholded images of Rab5 and Rab7 staining. To generate a
558 mask of Rab5/Rab7 double positive endosomes, the product of their individual masks was
559 used. The integrated fluorescence intensity of EGFR-mCherry was determined in each of
560 the endosomal masks and divided by the total integrated EGFR fluorescence intensity of
561 the cell. All analysis was performed using ImageJ. A cell segmentor tool was developed in-
562 house in Anaconda Python (Python Software Foundation, version 2.7,
563 https://www.python.org/) to quantify the spatial distribution of EGFR and pY845-EGFR in
564 fixed cells. Cells were divided into 6 equally spaced radial bins emanating from the centre
565 of cell mass.
566

567 *Confocal imaging*

568 Routinely, cells were cultured for live cell confocal imaging on 4- or 8-well chambered glass
569 slides (Lab-tek) and transiently transfected as described above. Confocal images were
570 recorded using an Olympus Fluoview FV1000 confocal microscope (Olympus Life Science
571 Europa, Hamburg, Germany) or a Leica SP8 confocal microscope (Leica Microsystems,
572 Wetzlar, Germany).

573

574 *Olympus Fluoview™ FV100*

575 The Olympus Fluoview™ FV1000 confocal microscope was equipped with a temperature
576 controlled CO_2 incubation chamber at 37°C (EMBL, Heidelberg, Germany) and a 60x/1.35
577 NA Oil UPLSApo objective (Olympus, Hamburg, Germany). EphA2-mCitrine and EGFR-
578 mCherry were excited using a 488 nm Argon-laser (GLG 3135, Showa Optronics, Tokyo,
579 Japan) and a 561 nm DPSS laser (85-YCA-020-230, Melles Griot, Bensheim, Germany),
580 respectively. Detection of fluorescence emission was restricted with an Acousto-Optical
581 Beam Splitter (AOBS) for mCitrine @ 498-551 nm and mCherry @ 575-675 nm. In all cases,
582 scanning was performed in frame-by-frame sequential mode with 2x frame averaging. The
583 pinhole was set to 250 µm.

584

585 *Leica SP8*

586 The Leica TCS SP8 confocal microscope was equipped with an environment-controlled
587 chamber (LIFE IMAGING SERVICES, Switzerland) maintained at 37°C and a HC PL APO CS2
588 1.4 NA oil objective (Leica Microsystems, Wetzlar, Germany). Alexa488-conjugated
589 secondary antibodies, fluorescent fusion proteins containing mCitrine and mCherry, and
590 EGF-Alexa647 were excited using a 470–670 nm white light laser (white light laser Kit
591 WLL2, NKT Photonics, Denmark) at 488, 514 and 561 and 647 nm, respectively. PH-Akt-
592 Cerulean was excited using an Argon Laser at 458 nm. Detection of fluorescence emission
593 was restricted with an AOBS as follows: Cerulean @ 468-505 nm, Alexa488 @ 498-551 nm,
594 mCitrine @ 525-570 nm, mCherry @ 570-650 nm and Alexa647 @ 654-754 nm. The
595 pinhole was set to 250 µm and 12-bit images of 512x512 pixels were acquired in a frame-
596 by-frame sequential mode.

597

598 *Analysis of time-lapse confocal imaging*

599

600 All analysis of live cell imaging data required an initial background subtraction for all
601 images obtained.

602

603 To quantify the proportion of endosomal EGFR-mCherry or EphA2-mCitrine, binary masks
604 of endosomes were generated from intensity thresholded images. The integrated
605 fluorescence intensity of EGFR-mCherry and EphA2-mCitrine was determined in their
606 corresponding endosomal masks and divided by the total integrated fluorescence intensity
607 of the cell.

608

609 Quantification of PM EGF-Alexa647 binding and PTB-mCherry translocation was
610 performed using the cell segmentation tool described above. To quantify PTB-mCherry
611 translocation to the PM, the mean intensity of the outermost, PM segment was divided by
612 the mean nuclear intensity. To determine the proportion of phosphorylated EGFR at the
613 PM, PM translocated PTB-mCherry was divided by the PM intensity of EGFR-mCitrine.

614

615 Photoactivation experiments were carried out at 37°C on a Leica SP8. EGFR-mCherry was
616 co-expressed to identify and select regions of endosomal EGFR for photoactivation.
617 Background intensity of EGFR-paGFP prior to photoactivation was measured and
618 subtracted from post-activation images. Photoactivation of EGFR-paGFP was performed
619 with the 405nm laser at 90% power. Following photoactivation, fluorescence images of
620 EGFR-paGFP were acquired every minute for a total of 15 minutes. PM EGFR-paGFP
621 fluorescence was quantified as the integrated intensity in a 5-pixel ring of the cell
622 periphery and, after subtracting pre-activation background intensity, was calculated as a
623 proportion of total EGFR-paGFP intensity.

624

625 To measure changes PM EGF-Alexa647 binding with time, binary masks of endosomal EGF-
626 Alexa647 were generated from intensity thresholded images and PM EGF-Alexa647
627 intensity was calculated by subtracting endosomal EGF-Alexa647 from total EGF-Alexa647
628 fluorescence intensity. The percent of PM EGF-Alexa-647 was calculated by dividing PM-

629 EGF-Alexa647 by total fluorescence intensity. Curves were fit with a one-phase exponential
630 decay in GraphPad Prism v6 (GraphPad Software, La Jolla, CA, USA) and grouped by their
631 rates of loss in PM EGF binding using the k-means clustering package in R (www.r-
632 project.org).
633
634 *Flow cytometry*
635 Cells were detached using accutase, centrifuged at 200g for 5 min and resuspended in
636 serum-free DMEM. Cells were fixed with 5% sucrose/Roti-Histofix (w/v) for 15 min at
637 37°C. Ice-cold methanol was added to 90% (v/v) for 30 min on ice. Cells were rinsed once
638 with 0.5% BSA/TBS (w/v) and incubated with Odyssey TBS blocking buffer (LI-COR
639 Biosciences) for 30 min at room temperature. Anti-phospho-Akt(Ser473)-Alexa647 (4075,
640 Cell Signalling Technology) was added directly to blocking buffer and incubated overnight
641 at 4°C. Anti-Akt-Alexa488 (2917, Cell Signalling Technology) was added for 2 h prior to
642 measurement. Samples were analyzed using the LSRII flow cytometer (BD Biosciences).
643 Alexa488 was excited with a 488nm laser and fluorescence emission was collected using a
644 505 nm LP dichroic and a 530/30 nm filter. Alexa647 was excited with 633 nm lasers and
645 fluorescence emission was collected using a 670/40 nm filter. Samples were analyzed using
646 FlowJo v10 (FlowJo, LLC, Ashland, OR, USA) to obtain single cell intensity measurements of
647 phospho- and total Akt. Population distributions of log(phospho/total Akt) were fitted with
648 a single Gaussian or a sum of two Gaussian distributions using GraphPad Prism.
649
650 *Cell migration*
651 MEF cells were seeded onto fibronectin-coated (F0895, Sigma, 1.25 ug/cm^2) 12 well
652 culture dishes (83.3921, Sarstedt, Nuembrecht, Germany) containing 2-well Culture-Inserts
653 (80209, ibidi) to create a cell-free area. Immediately before stimulation, inserts were
654 removed and cells were incubated with Hoechst to label nuclei. Wide field images were
655 acquired using an Olympus IX81 inverted microscope (Olympus, Hamburg, Germany)
656 equipped with a MT20 illumination system, a 4x/0.16 NA air objective and an Orca CCD
657 camera (Hamamatsu Photonics, Hamamatsu City, Japan). Transmission and fluorescence
658 images were acquired every 10 min for 16 h. The cell-free area created by the Culture-
659 Insert was cropped using ImageJ and defined as the migration region. Individual cells were

660 detected and tracked by their nuclear Hoechst staining as they travelled within the
661 migration region using the TrackMate ImageJ plugin (Tinevez et al. 2016), and the total
662 distance of each track was quantified.
663
664 *Immunoprecipitation (IP) and western blotting*
665 Cells were lysed in TGH (150 mM NaCl, 2 mM EGTA/EDTA, 50 mM HEPES (pH 7.4), 1%
666 Triton X-100, 10% glycerol, 1 mM phenylmethylsulfonyl fluoride, 10 mM N-
667 ethylmaleimide(NEM)) or RIPA (for immunoprecipitation; 50 mM Tris–HCl (pH 7.5), 150
668 mM NaCl, 1 mM EGTA, 1 mM EDTA, 1% Triton X-100, 1% Sodium deoxycholate, 0.2% SDS,
669 2.5 mM sodium pyrophosphate and 10 mM NEM), supplemented with Complete Mini
670 EDTA-free protease inhibitor (Roche Applied Science, Heidelberg, Germany) and 100 µl
671 phosphatase inhibitor cocktail 2 and 3 (P5726 and P0044, Sigma Aldrich). Lysates were
672 sonicated prior to centrifugation at 14 000 rpm for 10 min at 4°C to separate non-soluble
673 material. For immunoprecipitation, cell lysates were incubated with 50 µl washed Protein
674 G magnetic beads (10003D, Life Technologies) for 1 h at 4°C to pre-clear the samples from
675 unspecific binding proteins. Supernatants were incubated with primary antibody alone for
676 2 h followed by the addition and overnight incubation with Protein G magnetic beads at 4°C
677 with agitation. SDS–PAGE was performed using the X-cell II mini electrophoresis apparatus
678 (Life Technologies) according to the manufacturer's instructions. Samples were transferred
679 to preactivated PVDF membranes (Merck Millipore, Billerica, MA) and incubated with the
680 respective primary antibodies at 4°C overnight. Detection was performed using species-
681 specific secondary IR-Dye secondary antibodies (LI-COR Biosciences) and the Odyssey
682 Infrared Imaging System (LI-COR Biosciences). The integrated intensity of protein bands of
683 interest was measured using the ImageJ software and signals were normalised by dividing
684 the intensities of phosphorylated protein by total protein intensities or by dividing
685 intensities of co-immunoprecipitated proteins by the corresponding immunoprecipitated
686 protein.
687
688
689
690

691 *References:*

692

693 Arrieumerlou, Cécile, and Tobias Meyer. 2005. 'A Local Coupling Model and Compass
694 Parameter for Eukaryotic Chemotaxis', *Developmental Cell*, 8: 215-27.

695 Astin, Jonathan W., Jennifer Batson, Shereen Kadir, Jessica Charlet, Raj A. Persad, David
696 Gillatt, Jon D. Oxley, and Catherine D. Nobes. 2010. 'Competition amongst Eph
697 receptors regulates contact inhibition of locomotion and invasiveness in prostate cancer
698 cells', *Nature cell biology*, 12: 1194-204.

699 Bailly, Maryse, Frank Macaluso, Michael Cammer, Amanda Chan, Jeffrey E. Segall, and John S.
700 Condeelis. 1999. 'Relationship between Arp2/3 Complex and the Barbed Ends of Actin
701 Filaments at the Leading Edge of Carcinoma Cells after Epidermal Growth Factor
702 Stimulation', *The Journal of Cell Biology*, 145: 331-45.

703 Bailly, Maryse, Jeffrey Wyckoff, Boumediene Bouzahzah, Ross Hammerman, Vonetta
704 Sylvestre, Michael Cammer, Richard Pestell, and Jeffrey E. Segall. 2000. 'Epidermal
705 Growth Factor Receptor Distribution during Chemotactic Responses', *Molecular Biology*
706 *of the Cell*, 11: 3873-83.

707 Batlle, Eduard, Julinor Bacani, Harry Begthel, Suzanne Jonkheer, Suzanne Jonkeer, Alexander
708 Gregorieff, Maaike van de Born, Núria Malats, Elena Sancho, Elles Boon, Tony Pawson,
709 Steven Gallinger, Steven Pals, and Hans Clevers. 2005. 'EphB receptor activity
710 suppresses colorectal cancer progression', *Nature*, 435: 1126-30.

711 Baumdick, Martin, Yannick Brüggemann, Malte Schmick, Georgia Xouri, Ola Sabet, Lloyd
712 Davis, Jason W. Chin, and Philippe I. H. Bastiaens. 2015. 'EGF-dependent re-routing of
713 vesicular recycling switches spontaneous phosphorylation suppression to EGFR
714 signaling', *eLife*, 4.

715 Baumdick, Martin, Márton Gélleri, Chayasith Uttamapinant, Vàclav Bernek, Jason W. Chin, and
716 Philippe I.H. Bastiaens. 2017. 'Conformational EGFR sensor based on genetic code
717 expansion reveals the autocatalytic activation of EGFR'. *Manuscript in preparation*.

718 Boyd, Andrew W., Perry F. Bartlett, and Martin Lackmann. 2013. 'Therapeutic targeting of EPH
719 receptors and their ligands', *Nature Reviews Drug Discovery*, 13: 39-62.

720 Chan, A. Y., S. Raft, M. Bailly, J. B. Wyckoff, J. E. Segall, and J. S. Condeelis. 1998. 'EGF
721 stimulates an increase in actin nucleation and filament number at the leading edge of the
722 lamellipod in mammary adenocarcinoma cells', *Journal of Cell Science*, 111 (Pt 2): 199-
723 211.

724 Chinkers, M., J. A. McKanna, and S. Cohen. 1979. 'Rapid induction of morphological changes in
725 human carcinoma cells A-431 by epidermal growth factors', *The Journal of Cell Biology*,
726 83: 260-65.

727 Cortina, Carme, Sergio Palomo-Ponce, Mar Iglesias, Juan Fernández-Masip, Ana Vivancos,
728 Gavin Whissell, Mireia Humà, Nerea Peiró, Lourdes Gallego, Suzanne Jonkheer, Alice
729 Davy, Josep Lloreta, Elena Sancho, and Eduard Batlle. 2007. 'EphB–ephrin-B
730 interactions suppress colorectal cancer progression by compartmentalizing tumor cells',
731 *Nature genetics*, 39: 1376-83.

732 Daaka, Yehia, Louis M. Luttrell, Seungkirl Ahn, Gregory J. Rocca, Stephen S. G. Ferguson,
733 Marc G. Caron, and Robert J. Lefkowitz. 1998. 'Essential role for G protein-coupled
734 receptor endocytosis in the activation of mitogen-activated protein kinase', *Journal of*
735 *Biological Chemistry*, 273: 685-88.

736 Davis, S., N. W. Gale, T. H. Aldrich, P. C. Maisonpierre, V. Lhotak, T. Pawson, M. Goldfarb,
737 and G. D. Yancopoulos. 1994. 'Ligands for EPH-related receptor tyrosine kinases that
738 require membrane attachment or clustering for activity', *Science*, 266: 816-19.

739 DeFea, K. A., J. Zalevsky, Thoma, O. Déry, R. D. Mullins, and N. W. Bunnett. 2000. 'β-
740 Arrestin–Dependent Endocytosis of Proteinase-Activated Receptor 2 Is Required for
741 Intracellular Targeting of Activated Erk1/2', *The Journal of Cell Biology*, 148: 1267-82.

742 Duchek, Peter, and Pernille Rørth. 2001. 'Guidance of Cell Migration by EGF Receptor
743 Signaling During Drosophila Oogenesis', *Science*, 291: 131-33.

744 Ebner, Michael, Iva Lučić, Thomas A. Leonard, and Ivan Yudushkin. 2017. 'PI(3,4,5)P3
745 Engagement Restricts Akt Activity to Cellular Membranes', *Molecular cell*, 65: 416-
746 431000000.

747 El-Sibai, Mirvat, Peri Nalbant, Huan Pang, Rory J. Flinn, Corina Sarmiento, Frank Macaluso,
748 Michael Cammer, John S. Condeelis, Klaus M. Hahn, and Jonathan M. Backer. 2007.
749 'Cdc42 is required for EGF-stimulated protrusion and motility in MTLn3 carcinoma
750 cells', *Journal of Cell Science*, 120: 3465-74.

751 Er, Ekrem, Michelle C. Mendoza, Ashley M. Mackey, Lucia E. Rameh, and John Blenis. 2013.
752 'AKT facilitates EGFR trafficking and degradation by phosphorylating and activating
753 PIKfyve', *Science Signaling*, 6.

754 Ferrell, James E., Jr, and Sang Ha. 2014. 'Ultrasensitivity part II: multisite phosphorylation,
755 stoichiometric inhibitors, and positive feedback', *Trends in biochemical sciences*, 39:
756 556-69.

757 Ferrell, James E., and Eric M. Machleder. 1998. 'The Biochemical Basis of an All-or-None Cell
758 Fate Switch in Xenopus Oocytes', *Science*, 280.

759 Fortian, Arola, and Alexander Sorkin. 2014. 'Live-cell fluorescence imaging reveals high
760 stoichiometry of Grb2 binding to the EGF receptor sustained during endocytosis', *Journal*
761 *of cell science*, 127: 432-44.

762 Guglielmo, Di G. M., P. C. Baass, W. J. Ou, B. I. Posner, and J. J. Bergeron. 1994.
763 'Compartmentalization of SHC, GRB2 and mSOS, and hyperphosphorylation of Raf-1 by
764 EGF but not insulin in liver parenchyma', *The EMBO Journal*, 13: 4269-77.

765 Haj, Fawaz G., Peter J. Verveer, Anthony Squire, Benjamin G. Neel, and Philippe I. H.
766 Bastiaens. 2002. 'Imaging Sites of Receptor Dephosphorylation by PTP1B on the Surface
767 of the Endoplasmic Reticulum', *Science*, 295: 1708-11.

768 Harms, Brian D., Gina M. Bassi, Alan Horwitz, and Douglas A. Lauffenburger. 2005.
769 'Directional Persistence of EGF-Induced Cell Migration Is Associated with Stabilization
770 of Lamellipodial Protrusions', *Biophysical Journal*, 88: 1479-88.

771 Haugh, Jason M., and Tobias Meyer. 2002. 'Active EGF receptors have limited access to
772 PtdIns(4,5)P2 in endosomes: implications for phospholipase C and PI 3-kinase signaling',
773 *J. Cell Sci.*, 115.

774 Howe, Charles L., Janice S. Valletta, Alex S. Rusnak, and William C. Mobley. 2001. 'NGF
775 Signaling from Clathrin-Coated Vesicles Evidence that Signaling Endosomes Serve as a
776 Platform for the Ras-MAPK Pathway', *Neuron*, 32: 801-14.

777 Ibach, Jenny, Yvonne Radon, Márton Gelléri, Michael H. Sonntag, Luc Brunsveld, Philippe I. H.
778 Bastiaens, and Peter J. Verveer. 2015. 'Single Particle Tracking Reveals that EGFR
779 Signaling Activity Is Amplified in Clathrin-Coated Pits', *PLOS ONE*, 10.

780 Jékely, Gáspár, Hsin-Ho Sung, Carlos M. Luque, and Pernille Rørth. 2005. 'Regulators of
781 Endocytosis Maintain Localized Receptor Tyrosine Kinase Signaling in Guided
782 Migration', *Developmental Cell*, 9: 197-207.

783 Jethwa, Nirmal, Gary H. C. Chung, Marta G. Lete, Alicia Alonso, Richard D. Byrne, Véronique
784 Calleja, and Banafshé Larijani. 2015. 'Endomembrane PtdIns(3,4,5)P3 activates the
785 PI3K–Akt pathway', *J Cell Sci*, 128: 3456-65.

786 Konturek, J. W., W. Bielanski, S. J. Konturek, J. Bogdal, and J. Oleksy. 1989. 'Distribution and
787 release of epidermal growth factor in man', *Gut*, 30: 1194-200.

788 Laketa, Vibor, Sirus Zarbakhsh, Alexis Traynor-Kaplan, Aidan Macnamara, Devaraj
789 Subramanian, Mateusz Putyrski, Rainer Mueller, André Nadler, Matthias Mentel, Julio
790 Saez-Rodriguez, Rainer Pepperkok, and Carsten Schultz. 2014. 'PIP_3 induces the
791 recycling of receptor tyrosine kinases', *Science signaling*, 7.

792 Li, Guo, Xiao-Dan Ji, Hong Gao, Jiang-Sha Zhao, Jun-Feng Xu, Zhi-Jian Sun, Yue-Zhen Deng,
793 Shuo Shi, Yu-Xiong Feng, Yin-Qiu Zhu, Tao Wang, Jing-Jing Li, and Dong Xie. 2012.
794 'EphB3 suppresses non-small-cell lung cancer metastasis via a PP2A/RACK1/Akt
795 signalling complex', *Nature communications*, 3.

796 Li, J. J., D. P. Liu, G. T. Liu, and D. Xie. 2009. 'EphrinA5 acts as a tumor suppressor in glioma
797 by negative regulation of epidermal growth factor receptor', *Oncogene*, 28.

798 Li, Jing, Meei-Lih Lin, Gregory J. Wiepz, Arturo G. Guadarrama, and Paul J. Bertics. 1999.
799 'Integrin-mediated Migration of Murine B82L Fibroblasts Is Dependent on the
800 Expression of an Intact Epidermal Growth Factor Receptor', *Journal of Biological*
801 *Chemistry*, 274: 11209-19.

802 Lin, Benjamin, Taofei Yin, Yi I. Wu, Takanari Inoue, and Andre Levchenko. 2015. 'Interplay
803 between chemotaxis and contact inhibition of locomotion determines exploratory cell
804 migration', *Nature communications*, 6: 6619.

805 Macdonald, Jennifer L., and Linda J. Pike. 2008. 'Heterogeneity in EGF-binding affinities arises
806 from negative cooperativity in an aggregating system', *Proceedings of the National*
807 *Academy of Sciences*, 105: 112-17.

808 Maminska, A., A. Bartosik, Banach-Or M. owska, I. Pilecka, Jastrz K. bski, D. Zdzalik-Bielecka,
809 I. Castanon, M. Poulain, C. Neyen, Woli L. ska-Nizio, Szyma E. ska, A. Kowalczyk, K.
810 Piwocka, A. Simonsen, H. Stenmark, M. Furthauer, M. Gonzalez-Gaitan, and M.
811 Miaczynska. 2016. 'ESCRT proteins restrict constitutive NF- B signaling by trafficking
812 cytokine receptors', *Science signaling*, 9.

813 Masip, Martin E., Jan Huebinger, Jens Christmann, Ola Sabet, Frank Wehner, Antonios
814 Konitsiotis, Günther R. Fuhr, and Philippe I. H. Bastiaens. 2016. 'Reversible cryo-arrest
815 for imaging molecules in living cells at high spatial resolution', *Nature methods*, 13: 665-
816 72.

817 Matsuda, Miho, Hugh F. Paterson, Rosie Rodriguez, Amanda C. Fensome, Moira V. Ellis, Karl
818 Swann, and Matilda Katan. 2001. 'Real Time Fluorescence Imaging of Plcγ Translocation
819 and Its Interaction with the Epidermal Growth Factor Receptor', *The Journal of Cell*
820 *Biology*, 153: 599-612.

821 Ménard, Ludovic, Peter J. Parker, and Stéphanie Kermorgant. 2014. 'Receptor tyrosine kinase c-
822 Met controls the cytoskeleton from different endosomes via different pathways', *Nature*
823 *communications*, 5: 3907.

824 Merlos-Suárez, Anna, and Eduard Batlle. 2008. 'Eph–ephrin signalling in adult tissues and
825 cancer', *Current Opinion in Cell Biology*, 20: 194-200.

826 Miao, H., B. R. Wei, D. M. Peehl, Q. Li, T. Alexandrou, J. R. Schelling, J. S. Rhim, J. R. Sedor,
827 E. Burnett, and B. Wang. 2001. 'Activation of EphA receptor tyrosine kinase inhibits the
828 Ras/MAPK pathway', *Nature cell biology*, 3.

829 Miao, Hui, Da-Qiang Li, Amitava Mukherjee, Hong Guo, Aaron Petty, Jennifer Cutter, James P.
830 Basilion, John Sedor, Jiong Wu, David Danielpour, Andrew E. Sloan, Mark L. Cohen,
831 and Bingcheng Wang. 2009. 'EphA2 mediates ligand-dependent inhibition and ligand-
832 independent promotion of cell migration and invasion via a reciprocal regulatory loop
833 with Akt', *Cancer cell*, 16.

834 Nada, Shigeyki, Akihiro Hondo, Atsuko Kasai, Masato Koike, Kazunobu Saito, Yasuo
835 Uchiyama, and Masato Okada. 2009. 'The novel lipid raft adaptor p18 controls endosome

836 dynamics by anchoring the MEK–ERK pathway to late endosomes', *The EMBO Journal*,
837 28: 477-89.

838 Navenot, Jean-Marc, Nobutaka Fujii, and Stephen C. Peiper. 2009. 'KiSS1 metastasis suppressor
839 gene product induces suppression of tyrosine kinase receptor signaling to Akt, tumor
840 necrosis factor family ligand expression, and apoptosis', *Molecular pharmacology*, 75.

841 Nishimura, Yukio, Soichi Takiguchi, Shigeru Ito, and Kazuyuki Itoh. 2015. 'EGF‐stimulated
842 AKT activation is mediated by EGFR recycling via an early endocytic pathway in a
843 gefitinib‐resistant human lung cancer cell line', *International journal of oncology*, 46.

844 Pasquale, Elena B. 2010. 'Eph receptors and ephrins in cancer: bidirectional signalling and
845 beyond', *Nature Reviews Cancer*, 10: 165-80.

846 Poteryaev, Dmitry, Sunando Datta, Karin Ackema, Marino Zerial, and Anne Spang. 2009.
847 'Identification of the Switch in Early-to-Late Endosome Transition', *Cell*, 141: 497-508.

848 Reynolds, Andrew R., Christian Tischer, Peter J. Verveer, Oliver Rocks, and Philippe I. H.
849 Bastiaens. 2003. 'EGFR activation coupled to inhibition of tyrosine phosphatases causes
850 lateral signal propagation', *Nature Cell Biology*, 5: 447-53.

851 Ridley, Anne J., and Alan Hall. 1992. 'The small GTP-binding protein rho regulates the assembly
852 of focal adhesions and actin stress fibers in response to growth factors', *Cell*, 70: 389-99.

853 Sabet, Ola, Rabea Stockert, Georgia Xouri, Yannick Brüggemann, Angel Stanoev, and Philippe
854 I. H. Bastiaens. 2015. 'Ubiquitination switches EphA2 vesicular traffic from a continuous
855 safeguard to a finite signalling mode', *Nature communications*, 6: 8047.

856 Sadowski, Łukasz, Kamil Jastrzębski, Yannis Kalaidzidis, Carl-Henrik Heldin, Carina Hellberg,
857 and Marta Miaczynska. 2013. 'Dynamin Inhibitors Impair Endocytosis and Mitogenic
858 Signaling of PDGF', *Traffic*, 14: 725-36.

859 Schenck, Annette, Livia Goto-Silva, Claudio Collinet, Muriel Rhinn, Angelika Giner, Bianca
860 Habermann, Michael Brand, and Marino Zerial. 2008. 'The Endosomal Protein Appl1
861 Mediates Akt Substrate Specificity and Cell Survival in Vertebrate Development', *Cell*,
862 133: 486-97.

863 Schmid, Sandra L. 2017. 'Reciprocal regulation of signaling and endocytosis: Implications for
864 the evolving cancer cell', *J Cell Biol*, 216.

865 Segall, Jeffrey E., Sangeeta Tyerech, Lucia Boselli, Susan Masseling, Joseph Helft, Amanda
866 Chan, Joan Jones, and John Condeelis. 1996. 'EGF stimulates lamellipod extension in
867 metastatic mammary adenocarcinoma cells by an actin-dependent mechanism', *Clinical*
868 *& Experimental Metastasis*, 14: 61-72.

869 Sigismund, Sara, Veronica Algisi, Gilda Nappo, Alexia Conte, Roberta Pascolutti, Alessandro
870 Cuomo, Tiziana Bonaldi, Elisabetta Argenzio, Lisette G. G. C. Verhoef, Elena Maspero,
871 Fabrizio Bianchi, Fabrizio Capuani, Andrea Ciliberto, Simona Polo, and Pier Fiore. 2013.

872 'Threshold-controlled ubiquitination of the EGFR directs receptor fate', *The EMBO*
873 *Journal*, 32: 2140-57.

874 Sorkin, Alexander, and Mark von Zastrow. 2009. 'Endocytosis and signalling: intertwining
875 molecular networks', *Nature Reviews Molecular Cell Biology*, 10: 609-22.

876 Stanoev, Angel, Amit Mhamane, Klaus C. Schuermann, Hernán Grecco, Sven Fengler, Pedro
877 Roda-Navarro, Rabea Stockaert, Maitreyi S. Joshi, Yannick Brüggemann, Lisaweta
878 Roßmannek, Jutta Luig, Aneta Koseska, and Philippe I.H. Bastiaens. 2017.
879 'Interdependence of EGFR with PTPs on juxtaposed membranes generates a growth
880 factor sensing network', *In revision.*

881 Teis, David, Nicole Taub, Robert Kurzbauer, Diana Hilber, Mariana E. de Araujo, Miriam
882 Erlacher, Martin Offterdinger, Andreas Villunger, Stephan Geley, Georg Bohn, Christoph
883 Klein, Michael W. Hess, and Lukas A. Huber. 2006. 'p14-MP1-MEK1 signaling
884 regulates endosomal traffic and cellular proliferation during tissue homeostasis', *The*
885 *Journal of Cell Biology*, 175: 861-68.

886 Tinevez, Jean-Yves, Nick Perry, Johannes Schindelin, Genevieve M. Hoopes, Gregory D.
887 Reynolds, Emmanuel Laplantine, Sebastian Y. Bednarek, Spencer L. Shorte, and Kevin
888 W. Eliceiri. 2016. 'TrackMate: an open and extensible platform for single-particle
889 tracking', *Methods*.

890 Verma, Nandini, Omer Keinan, Michael Selitrennik, Thomas Karn, Martin Filipits, and Sima
891 Lev. 2015. 'PYK2 sustains endosomal-derived receptor signalling and enhances
892 epithelial-to-mesenchymal transition', *Nature communications*, 6: 6064.

893 Villaseñor, Roberto, Yannis Kalaidzidis, and Marino Zerial. 2016. 'Signal processing by the
894 endosomal system', *Current Opinion in Cell Biology*, 39: 53-60.

895 Villaseñor, Roberto, Hidenori Nonaka, Perla Conte-Zerial, Yannis Kalaidzidis, and Marino
896 Zerial. 2015. 'Regulation of EGFR signal transduction by analogue-to-digital conversion
897 in endosomes', *eLife*, 4.

898 Wouters, Fred S., and Philippe Bastiaens. 1999. 'Fluorescence lifetime imaging of receptor
899 tyrosine kinase activity in cells', *Current Biology*, 9: 1127.

900 Yarden, Yosef, and Mark X. Sliwkowski. 2001. 'Untangling the ErbB signalling network',
901 *Nature Reviews Molecular Cell Biology*, 2: 127-37.

902 Yip, Shu-Chin, Mirvat El-Sibai, Salvatore J. Coniglio, Ghassan Mouneimne, Robert J. Eddy,
903 Beth E. Drees, Paul O. Neilsen, Sumanta Goswami, Marc Symons, John S. Condeelis,
904 and Jonathan M. Backer. 2007. 'The distinct roles of Ras and Rac in PI 3-kinase-
905 dependent protrusion during EGF-stimulated cell migration', *Journal of Cell Science*,
906 120: 3138-46.

907 Yuan, Tina L., Gerburg Wulf, Laura Burga, and Lewis C. Cantley. 2011. 'Cell-to-Cell Variability
908 in PI3K Protein Level Regulates PI3K-AKT Pathway Activity in Cell Populations',
909 *Current Biology*, 21: 173-83.

910 Yudushkin, Ivan A., Andreas Schleifenbaum, Ali Kinkhabwala, Benjamin G. Neel, Carsten
911 Schultz, and Philippe I. H. Bastiaens. 2007. 'Live-Cell Imaging of Enzyme-Substrate
912 Interaction Reveals Spatial Regulation of PTP1B', *Science*, 315: 115-19.
913

914

915 **Figure Legends:**

916

917 **Figure 1: Akt-dependent recycling of EGFR sustains its autocatalytic activation at the**
918 **PM**. **(a)** Representative images of Cos-7 cells expressing EGFR-mCherry before (top left)
919 and after (top right) treatment with the Akt inhibitor AktVIII (10 μM, 1 h) and
920 quantification of the increase in endosomal EGFR-mCherry during AktVIII treatment (*N* =
921 6). See also Supplementary Movie 1. **(b)** Quantification of PM EGFR abundance by On-cell
922 Western (OCW, top) and Akt activation by In-cell Western (ICW, bottom) following
923 treatment with AktVIII for the times indicated. **(c)** Immunofluorescence measurements of
924 EGFR intensity in Rab5-, Rab5/Rab7- and Rab7-positive endosomal compartments as a
925 proportion of total EGFR intensity in DMSO (control, white, *N* = 6) and AktVIII (orange, *N* =
926 11) treated conditions, as well as DMSO- (red, *N* = 9) and AktVIII-pretreated (green, *N* = 8)
927 conditions followed by EGF stimulation (100 ng/ml, 1 h). **(d)** Quantification of PM EGFR
928 abundance and Akt activation by OCW and ICW, respectively, following treatment with the
929 PP2A inhibitor okadaic acid (OA, 1 μM, 2 h). **(e)** Measurements of EGFR-paGFP recycling to
930 the PM following photoactivation in endosomes (top) in control (gray, *N* = 10), EGF (20
931 ng/ml, 15 min, red, *N* = 6), AktVIII (orange, *N* = 9) and AktVIII-pretreated, EGF-stimulated
932 (green, *N* = 8). **(f,g)** ICW measurements of total EGFR abundance (f) and phosphorylation
933 (g) following EGF stimulation (1-200 ng/ml, 30 min) in DMSO (control, gray) and AktVIII
934 (orange) pretreated cells. EGFR phosphorylation was measured using antibodies
935 recognizing phosphorylated Y_{845} (g, top), Y_{1068} (g, middle) and Y_{1045} (g, bottom). **(h,i)** Live
936 cell measurements of EGF-Alexa647 binding to the PM (green) and PTB-mCherry
937 translocation to the PM (magenta) with increasing EGF-Alexa647 concentrations (1, 3, 10
938 and 20 ng/ml, as indicated) for 2 min each in control (h, *N* = 9) and AktVIII-pretreated (i, *N*
939 = 7) cells. **(j)** Comparison of PTB-mCherry translocation for equivalent numbers of
940 liganded receptors for data presented in h,i. **(k)** Spatial-temporal maps of EGFR abundance
941 (top) and Y_{845} phosphorylation (bottom) obtained by immunofluorescence in radially
942 segmented cells (plasma membrane, PM → nuclear membrane, NM) prior to and after EGF
943 stimulation (20 ng/ml for 5, 30 and 60 min) in control (left), AktVIII- (middle) and
944 YM201636- (YM, 200 nM, 1 h) pretreated cells (*N* = 50-90 cells per condition). **(l)** Spatial

945 network topology showing positive feedback generated by coupling PM EGFR activity and
946 Akt-dependent vesicular trafficking. PIKfyve inhibition by YM decouples Akt activation
947 from its effect on EGFR recycling. All experiments were performed in Cos-7 cells. Data in c
948 are represented by Tukey boxplots with the mean denoted as a cross and the median as a
949 line. All other data represents means ± s.e.m. Statistical significance was determined in c
950 using an ordinary one-way ANOVA with Sidak's multiple corrections *post-hoc* test, in d
951 using a Student's *t* test and in f,g using a two-way ANOVA with Sidak's multiple corrections
952 *post-hoc* test (***, $p > 0.001$; **, $p > 0.01$; *, $p > 0.05$). Scale bars = 20 μm
953
954

955 **Figure 2: Eph receptor activation regulates EGFR vesicular trafficking. (a)**
956 Representative images of Cos-7 cells expressing EGFR-mCherry and EphA2-mCitrine
957 (green and magenta in merged images, respectively) following stimulation with EphrinA1-
958 Fc (A1, 2 μg/ml). See Supplementary Movie 2. **(b)** Quantification of endosomal EphA2-
959 mCitrine and EGFR-mCherry from time-lapse confocal imaging during A1 stimulation (*N* =
960 7). **(c)** Immunofluorescence measurements of EGFR intensity in Rab5-, Rab5/Rab7- and
961 Rab7-positive endosomal compartments as a proportion of total EGFR intensity in control
962 (white, *N* = 6) and A1 treated (60 min, magenta, *N* = 9) **(d)** Quantification of PM EphA2 and
963 EGFR abundance by OCW during A1 treatment. **(e)** Cos-7 lysates immunoprecipitated (IP)
964 with anti-EGFR (left) or blotted for total proteins (right) following stimulation with EGF
965 (100 ng/ml) or A1 for the indicated times. IP was probed with anti-HA (to detect co-
966 transfected HA-ubiquitin), anti-pY845, anti-pY1068, anti-pY1045 and anti-EGFR. Lysates
967 were probed with anti phospho-Eph (pEph), anti-EphA2, anti-pY1068, anti-EGFR and anti-
968 tubulin. Shown are representative blots from three independent experiments. **(f)**
969 Measurements of EGFR recycling in control (gray) and A1-pretreated cells (green).
970 PM/total EGFR was quantified by immunofluorescence prior to (pre), after 15 min EGF
971 stimulation (10 ng/ml) and 15 min following EGF washout (*N* = 34-40 cells/condition). All
972 experiments were performed in Cos-7 cells. Data in c are represented by Tukey boxplots
973 with the mean denoted as a cross and the median as a line. All other data represents means
974 ± s.e.m. Statistical significance was determined in c using an ordinary one-way ANOVA with
975 Sidak's multiple corrections *post-hoc* test and in d using a two-way ANOVA with Dunnett's
976 multiple corrections *post-hoc* test. Scale bars = 20 μm
977

978 **Figure 3: Cell-cell contact alters the spatial distribution of EGFR activity. (a)** Spatial-
979 temporal maps of EGFR abundance (top) and Y_{845} phosphorylation (bottom) in radially
980 segmented cells (plasma membrane, PM → nuclear membrane, NM) obtained by
981 immunofluorescence prior to and after EGF stimulation (20 ng/ml for 5, 30 and 60 min) in
982 control (left) and EphrinA1-Fc (A1, 2 μg/ml, 1 h) pretreated Cos-7 cells (*N* = 53-90 cells per
983 condition). Control data previously presented in Figure 1k. **(b)** Quantification of Akt and
984 ERK activation by ICW in control (gray) and A1-pretreated (1 h, green) Cos-7 cells
985 following EGF stimulation (1 ng/ml). **(c)** Quantification of Akt activation by ICW in HEK293
986 cells pretreated for 1 h with vehicle (control, gray) or A1 (green), followed by 30 min
987 treatment with the dynamin inhibitor dynole 34-2 (100 μM, 30 min, top) or its negative
988 control analog dynole 31-2 (bottom), then stimulated with EGF (1 ng/ml) for the times
989 indicated. **(d)** Quantification of EGF-promoted Akt activation by ICW following
990 pretreatment with increasing concentrations of A1 (0.02, 0.2 and 2 μg/ml, 1 h) in Cos-7
991 cells. **(e,f)** Single cell measurements of Akt (e) and ERK (f) activation versus cell-cell
992 contact in 2-D cultures (% cell circumference) in control (gray) and EGF stimulated (20
993 ng/ml, 1 h, blue) Cos-7 cells. **(g)** Quantification of Akt activation (pink) and PM EGFR
994 abundance (magenta) in HEK293 cells by ICW and OCW, respectively, following stimulation
995 with kisspeptin-10 (Kp-10, 100 nM). **(h,i)** Quantification of Akt and ERK activation by ICW
996 for control (gray) and Kp-10-pretreated (1 h, magenta) HEK293 cells following EGF
997 stimulation (1 ng/ml). **(j,k)** Single cell measurements of Akt phosphorylation by flow
998 cytometry in control (top), YM201636- (YM, 200 nM, 1h, middle) and EphrinA1-Fc- (A1, 2
999 μg/ml, 1h, bottom) pretreated Cos-7 cells following stimulation with the EGF
1000 concentrations indicated (ng/ml, 1 h). (j) Solid lines represent the sum of two Gaussian fits
1001 for data accumulated from at least 10 000 cells per condition in 3-4 independent
1002 experiments. (k) Quantification of Akt activation for increasing concentrations of EGF.
1003 Circle sizes represent the relative proportions of the low (gray) and high (red) Akt activity
1004 populations from the Gaussian distributions derived for each EGF concentration shown in j.
1005 **(l)** Quantification of PM EGF as a percent of total EGF intensity from time lapse imaging.
1006 Individual Cos-7 cells (thin lines) were clustered by their rate of PM EGF loss into two
1007 distinct groups (1, green; 2, magenta; group mean represented by thick line). (m) Rate of

1008 loss of PM EGF binding for individual cells in each group (mean ± s.d.). All other data
1009 represents means ± s.e.m. Statistical significance was determined using a Student's *t* test.
1010 **(n)** Percent of cells in group 1 (green) and 2 (magenta) for control and A1-pretreated
1011 conditions.
1012
1013

1014 **Figure 4: Cell-cell contact changes the cellular outcome of EGF stimulation. (a)**
1015 Percent of NIH 3T3 cells initiating a migratory response (top, means ± s.e.m) and the
1016 distance travelled by migratory cells (bottom, means ± s.d.) following EGF stimulation. Cells
1017 were pretreated with vehicle (control, blue), YM201636 (YM, 200 nM, 1 h, purple), or
1018 EphrinA1-Fc (A1, green: 2 μg/ml, 1h, or red: 0.02-2 μg/ml as indicated) followed by EGF
1019 stimulation (0-100 ng/ml as indicated) and tracked for 16 h. See Supplementary Movie 4.
1020 **(b)** NIH 3T3 cells were seeded at low and high density in a single well, separated by a
1021 removable insert. Following pretreatment with vehicle or A1 (2 μg/ml, 1 h), cells were
1022 stimulated with EGF (20 ng/ml) and tracked for 16 h (means ± s.e.m). (c) Quantification of
1023 retinoblastoma (Rb) phosphorylation by ICW for vehicle- (control, blue), A1- (green) and
1024 YM- (magenta) pretreated NIH 3T3 cells following 24 h EGF stimulation at the
1025 concentrations indicated (means ± s.e.m). Data in a and b were obtained from least three
1026 independent experiments, consisting of at least two replicates per experiment (N = 581 –
1027 1483 cells/condition). Statistical significance in a and b was determined using an ordinary
1028 one-way ANOVA with Holm-Sidak's multiple corrections *post-hoc* test.
1029

Figure 1: Akt-dependent recycling of EGFR sustains its autocatalytic activation at the PM.

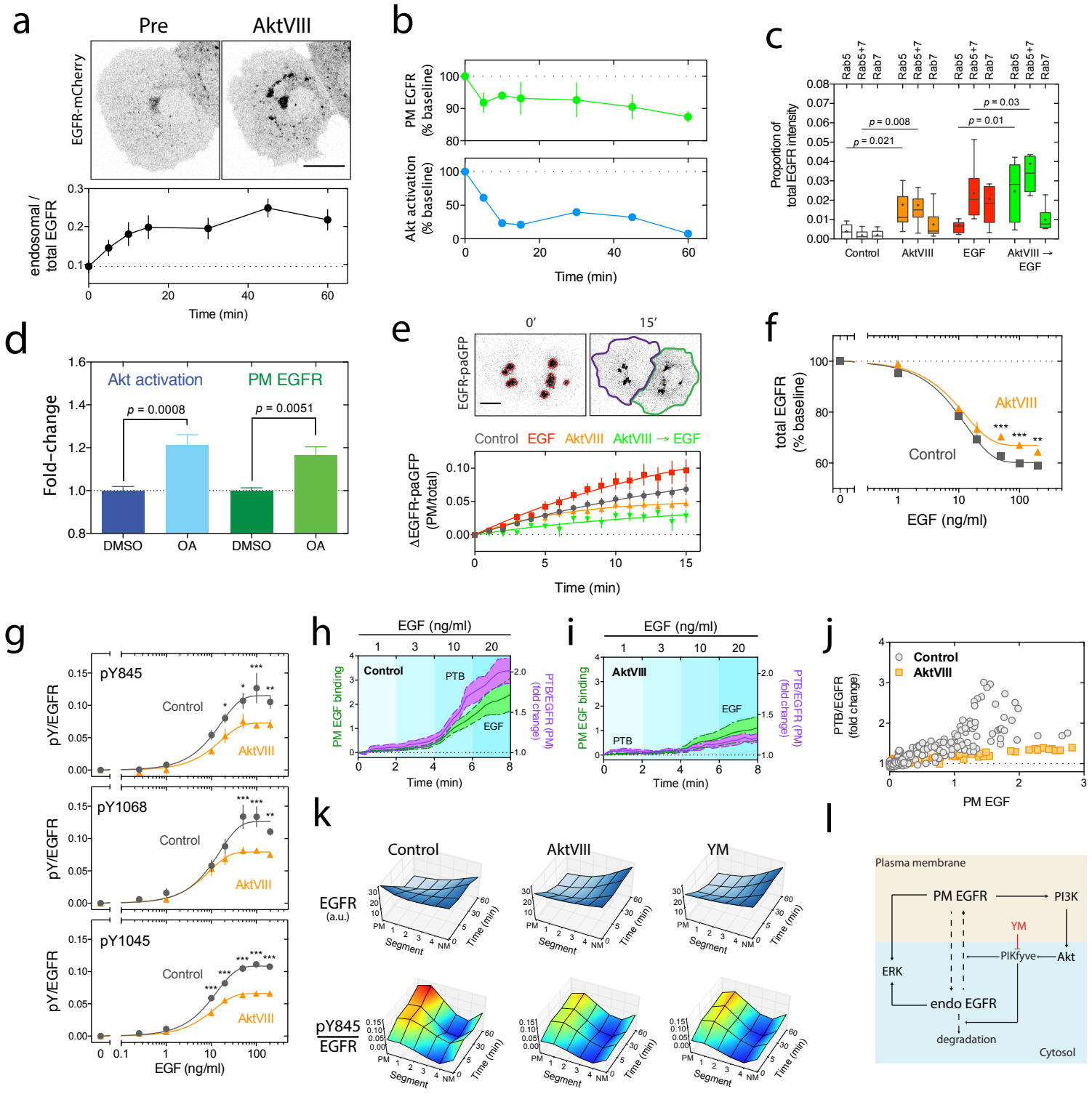

Figure 2: Eph receptor activation regulates EGFR vesicular trafficking.

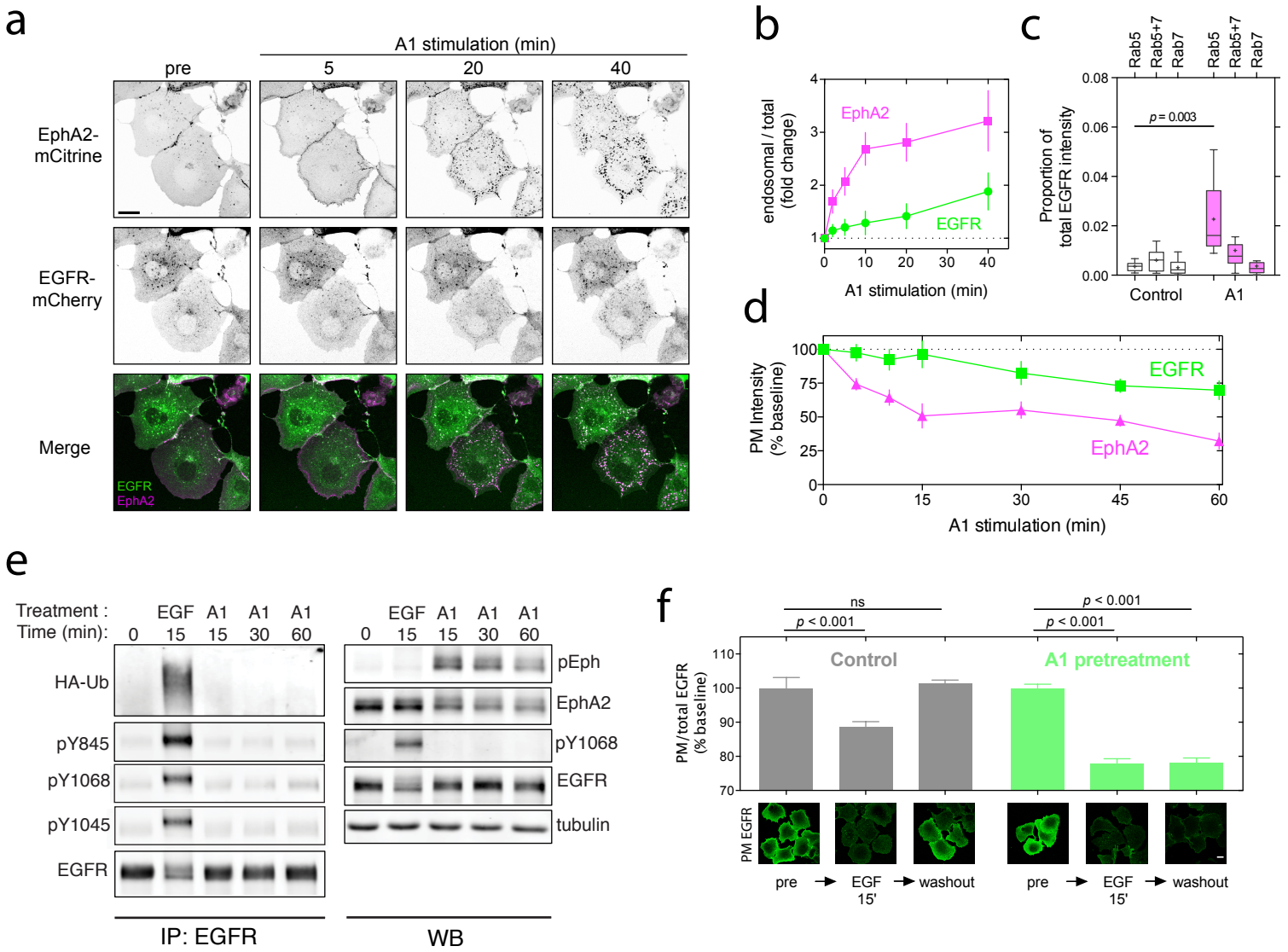

Figure 3: Cell-cell contact alters the spatial distribution of EGFR activity.

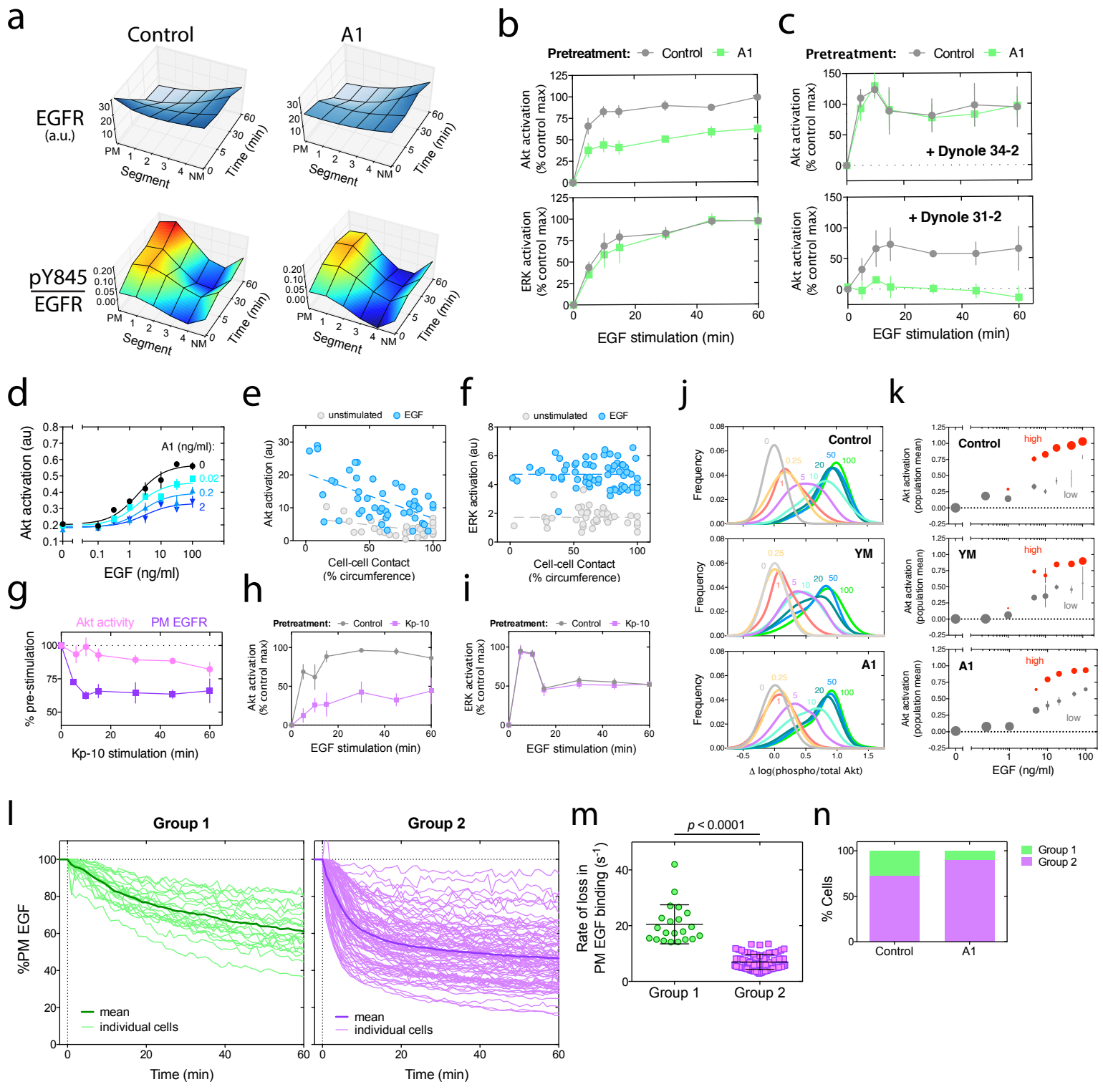
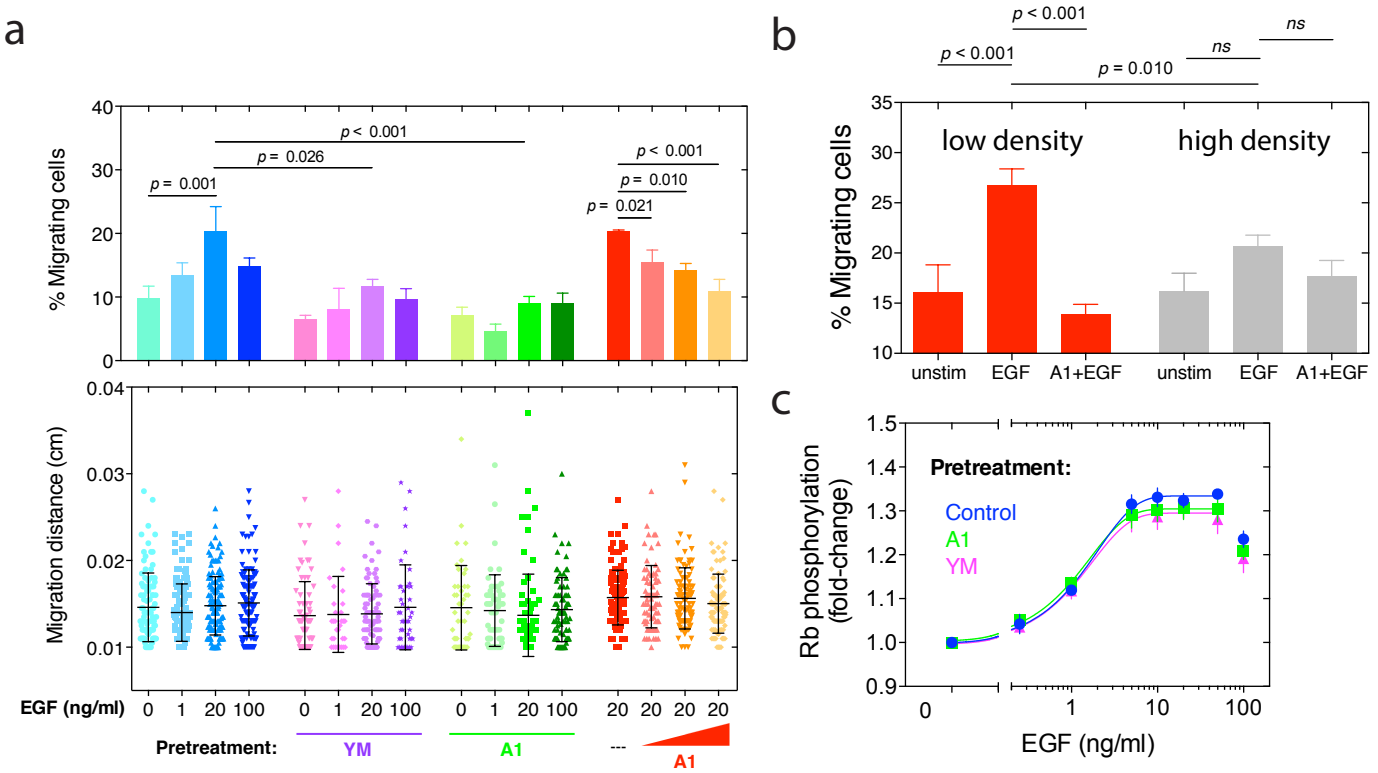
Figure 4: Cell-cell contact changes the cellular outcome of EGF stimulation.